Ab initio studies of solid bromine under high pressure

Defang Duan, Yanhui Liu, Yanming Ma, Zhiming Liu, Tian Cui,* Bingbing Liu, and Guangtian Zou
National Laboratory of Superhard Materials, Jilin University, Changchun 130012, People's Republic of China
(Received 29 April 2007; revised manuscript received 31 July 2007; published 26 September 2007)

Crystal structures of bromine under high pressure have been studied by employing plane-wave pseudopotential method with the generalized gradient approximation. It is found that the band overlap in the molecular *Cmca* phase, which causes the pressure-induced insulator-to-metal transition, occurs at about 55 GPa. Geometry optimization shows that the bromine changes to a face-centered orthorhombic (fco) phase with equal interatomic distances $d_1=d_2=d_3$ at about 75 GPa, but this fco structure is mechanically unstable with shear elastic stiffness coefficient $C_{66}<0$. For understanding the structure of this phase, we have modeled an incommensurate structure by a rational approximation with modulation vector $k=(0.25,0,0)$ according to the previous research results in solid iodine. Our results show that the enthalpy of this modulated phase is lower than that of the fco solid, and the elastic stiffness coefficients (C_{ij}) satisfy the Born stability criteria, indicating that the modulated structure is more thermodynamically stable and mechanically stable. In addition, through comparing the x-ray diffraction patterns of our structure with the experimental one, we conclude that the structure of bromine phase V is close to our modulated structure. It is clearly illustrated that the phase transition from *Cmca* phase to the incommensurate phase is associated with the instability of the shear elastic stiffness coefficient C_{44} which is related to the softening of the long-wavelength part of the transverse branch near the center of the first Brillouin zone. With the increasing of pressure, the modulated phase transforms into the monatomic phase II with body-centered orthorhombic structure at about 100 GPa, which is in agreement with the experimental result.

DOI: 10.1103/PhysRevB.76.104113 PACS number(s): 61.50.Ks, 61.50.Ah

I. INTRODUCTION

Development of high-pressure techniques led many interesting structures appearing in the past decade. For instance, discoveries of the incommensurate composite structures of Ba, As, Sb, and Bi[1–3] and the incommensurately modulated structures in group VI elements Te, Se, and S[4–7] at high pressure have suggested that incommensurate structures of element materials are common under high pressure. The incommensurately modulated structures have also been observed in iodine[8] and bromine[9] under high pressure. For iodine, an incommensurate structure (phase V) was discovered at 23 GPa between the molecular phase I and the monatomic phase II by high-pressure x-ray diffraction study. This structure is approximately formed by modulating the face-centered orthorhombic (fco) structure with the modulation wave propagating along the *a* axis. According to the harmonic modulation wave, atoms are displaced from their ideal positions along the *b* axis. Upon compression, the fco distortion of iodine decreases and the incommensurate structure approaches the body-centered orthorhombic (bco) structure (monatomic phase II) at about 30 GPa. An amplitude mode, peculiar to the incommensurate phase, was clearly found for bromine and iodine by Raman scattering experiment.[9] An incommensurate phase of solid bromine was suggested at a pressure region above 80 GPa, and the monatomic phase II for bromine was estimated occurring around 115 GPa. However, the most recent x-ray-absorption experiment shows that the incommensurately modulated structure occurs at 65±5 GPa.[10] Up to now, there is no experimental x-ray diffraction study for Br-V, and the structure of the incommensurate phase is not clear. In this paper, we focus on the structure of this phase and related phase transitions using *ab initio* studies.

Each of solid iodine, bromine, and chlorine forms a diatomic molecular crystal with the base-centered-orthorhombic structure (*Cmca* symmetry) with four (two) diatomic molecules in the conventional (primitive) unit cell. This structure is layered with the molecules lying in the planes perpendicular to the *a* axis, as shown in Fig. 1(a). The red atoms are located in the $x=0$ plane, while the gray atoms are in the $x=1/2$ plane. The metallization of iodine was observed at 16 GPa (Ref. 11) without any structural change. For solid bromine, Fujihisa *et al.* reported[12] that the surface of crystal started to reflect light at 60 GPa, indicating an insulator-to-metal transition. With further application of pressure, the intermolecular distances become comparable to the intramolecular distance, where the molecular dissociation is attained. Recently, the first molecular dissociation to phase V was observed in iodine at 23 GPa (Ref. 8) and in bromine at 84 GPa by Raman scattering[9] or 65 GPa by x-ray absorption.[10] However, it is difficult to decide whether phase V has molecular or monatomic character. Further molecular dissociation made the intermediate phase V transform to the monatomic phase II at 30 and 115 GPa for iodine and bromine, respectively.[8,9] The crystal structure of the monatomic phase II was determined to be body-centered orthorhombic with two atoms in a unit cell with space group *Immm*. For iodine, phase II further transforms to a body-centered tetragonal phase (phase III) at 43 GPa.[13] A face-centered cubic phase (phase IV) was reported at 55 GPa,[14] and this phase persists to at least 276 GPa.[15] A similar scheme of phase transformations can be expected for bromine, but experimental results are much scarcer than those in the iodine case, which restricts our understanding of the nature of bromine under high pressure. *Ab initio* calculation for determining crystal structure is believed to be sufficiently accurate and

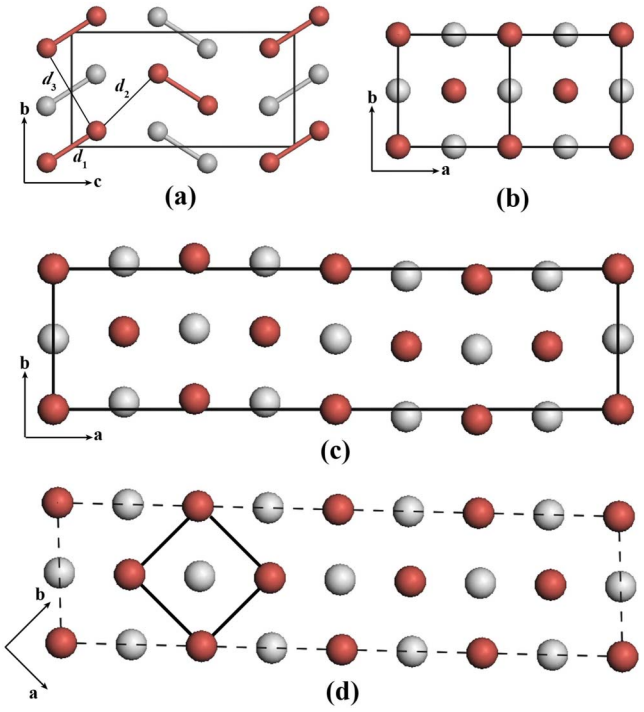

FIG. 1. (Color online) The crystal structures of solid bromine. The crystallographic unit cells are shown with solid rectangles. (a) Molecular phase I (*Cmca*). Red atoms are located in the $x=0$ plane, and gray atoms in the $x=1/2$ plane. (b) Face-centered orthorhombic structure. (c) Intermediate phase V with commensurately modulated structure. (d) High-pressure monatomic phase II (*Immm*). Red atoms are located in the $z=0$ plane and gray atoms in the $z=1/2$ plane in (b)–(d).

can provide additional information on ultrahigh-pressure structure.

Several theoretical studies for iodine and bromine have been reported.[16–19] The band overlap in the molecular phase has been investigated by detailed band calculations on the basis of the linear combination of atomic orbital picture.[16] The A_g modes, hyperfine parameters for both iodine and bromine molecular crystals, have been studied using the full-potential linear-muffin-tin-orbital method with the local density approximation.[17,18] In this work, the pressure-induced softening of the Raman active librational A_g is reproduced. Recently, the molecular crystal structure and the molecular dissociation of iodine, bromine, and chlorine under high pressure have been investigated by using the pseudopotential plane-wave method with local density approximation (LDA) and generalized gradient approximation (GGA).[19] However, little is known on the mechanical behavior when phase transitions happen, which is important for understanding structural stability and the mechanism of the phase transition from *Cmca* phase to incommensurate phase especially. In this paper, we have found that the shear elastic stiffness coefficient C_{44} of the *Cmca* phase softens to zero at about 75 GPa, indicating that the *Cmca* structure at that pressure becomes unstable and a phase transition happens. In addition, we have modeled an incommensurate phase with modulated structure according to the previous research results in solid iodine. On the basis of a comparison of x-ray diffraction patterns, enthalpy, and elastic stiffness coefficients, we suggest that the structure of the Br-V is closely similar to the modulated structure mimicked.

The organization of the paper is as follows. In Sec. II, our computational details are described; in Sec. III our results are shown and related discussions are made. Finally, in Sec. IV, we summarize our results.

II. COMPUTATIONAL METHOD

In our calculation, *ab initio* pseudopotential plane-wave density functional method implemented in the CASTEP code[20] has been used. All the possible structural optimizations in this paper including the atomic positions and the lattice constants are performed by the BFGS algorithm (proposed by Broyden, Fletcher, Goldfarb, and Shannon),[21] which provides a fast way of finding the lowest energy structure and the optimized cell. The optimization is not finished until the forces on the atoms are less than 0.01 eV/Å and all the stress components are less than 0.02 GPa. The tolerance in the self-consistent field (SCF) calculation is 5×10^{-7} eV/atom. The norm-conserving scheme is used to generate the pseudopotential with electronic configuration of $4s^24p^5$. The core radius is chosen as 1.89 a.u. for *s* and *p* orbitals. Exchange and correlation effects are described in the scheme of Perdew-Burke-Ernzerhof GGA.[22] The summation over the Brillouin zone has been performed with weighted summation over wave vectors generated by the Monkhorst-Pack scheme.[23] Convergence tests give a 0.03 $Å^{-1}$ grid spacing and 420 eV energy cutoff. With such a choice, the error bars of total energies are about 0.2 meV per atom. Elastic stiffness coefficients are evaluated from the linear relationship (Hooke's law) between the resultant stress and applied strain. The accuracy of the elastic constants, especially of the shear elastic constants, strongly depends on the quality of the SCF calculation and, in particular, on the quality of the Brillouin zone sampling and the degree of convergence of wave functions. So, when calculating the elastic constants, we use the **k**-space grid spacing $\Delta\mathbf{k}=0.02$ $Å^{-1}$ and a more precisely derived fast Fourier transform grid.

III. RESULTS AND DISCUSSIONS

A. Geometries under zero pressure and the equation of state

The smallest separation between two bromine molecules at 0 GPa in the different planes is comparable with the van der Waals diameter (4.02 Å),[24] indicating that the interaction between different planes is dominated by van der Waals-type potential. On the other hand, the interaction inside one molecular plane is more complicated. The intramolecular interaction is covalent while the intermolecular distances (3.31 and 3.79 Å) (Ref. 25) are shorter than the van der Waals diameter, which suggests that the interactions are partially covalent in character.[26]

The calculated lattice parameters under zero pressure, bulk modulus (B_0), and the pressure derivative (B_0') with GGA and LDA together with the experimental data and the previously theoretical results are listed in Table I. The lattice constants *b* and *c* and the neighboring distances d_1, d_2, and

TABLE I. The calculated lattice parameters, bulk modulus (B_0) and the pressure derivative of bulk modulus (B_0') of bromine crystal at 0 GPa. d_1 is the nearest-neighboring distance, i.e., bond length, d_2 and d_3 are the interatomic distances between the neighboring molecules in the same molecular plane. The results of experiment (Ref. 12) and previously theoretical calculation (Ref. 19) are also shown for comparison. Volumes are in $Å^3$, lattice constants and the interatomic distances are in Å, bulk modulus are in GPa.

Solid bromine		a	b	c	d_1	d_2	d_3	V	B_0	B_0'
Our results	GGA (0 GPa)	8.48	4.37	8.76	2.312	3.232	3.793	325.15	15.2	4.41
	GGA (0.2 GPa)	7.84	4.33	8.73	2.314	3.206	3.750	296.62		
	LDA	6.58	3.93	8.45	2.353	2.962	3.378	218.92	17.22	6.41
Ref. 19	GGA	6.753	4.292	8.412	2.35	3.14	3.66	318.72	16.24	3.38
	LDA	5.997	3.894	8.388	2.37	2.92	3.34	213.09	18.8	3.48
Experimental data		6.67[a]	4.48[a]	8.72[a]	2.27[a]	3.31[a]	3.79[a]	260.57[a]	14.1[b]	4.6[b]

[a]Reference 25.
[b]Reference 12.

d_3 within GGA are in good agreement with experimental data within 2.45%, 0.46%, 1.85%, 2.36%, and 0.08%. However, the lattice constant a and volume V are overestimated by 27.13% and 24.78%, respectively. The calculated volume at zero pressure is much larger than the experimental one due to the overestimation of the lattice constant a (interplanar distance). Indeed, while we apply a very small external pressure of 0.2 GPa, a and V decrease drastically and become 17.5% and 13.8% larger than the experimental values. The overestimation of lattice constant a is mainly attributed to that the van der Waals interaction between the molecular planes could not be described well by GGA. In case of the LDA, the lattice constant b and the neighboring distances d_1, d_2, and d_3 are underestimated by 12.3%, 8.3%, 10.5%, and 10.8%. Comparing the results of GGA with LDA, we choose the GGA in the following calculations.

The equation of state (EOS) of the *Cmca* phase is determined by fitting the pressure as a function of volume to the third-order Birch-Murnahan EOS,[27] which takes the form

$$P = \frac{3}{2}B_0\left[\left(\frac{V_0}{V}\right)^{7/3} - \left(\frac{V_0}{V}\right)^{5/3}\right]\left\{1 + \frac{3}{4}(4 - B_0')\times\left[\left(\frac{V_0}{V}\right)^{2/3} - 1\right]\right\}. \quad (1)$$

As discussed above, we have not obtained a good equilibrium volume at 0 GPa. Therefore, we use the experimental volume at zero pressure as V_0 to fit the EOS. The calculated EOS of the bromine within GGA is compared with the experimental data in Fig. 2. Note that the calculated EOS is in agreement with the experimental data.

B. Pressure-induced phase transitions

Geometry optimizations are performed with full structural relaxation including atomic positions and lattice constants to detect possible signals of structural phase transformations induced by pressure. Our results show that the *Cmca* structure changes to a face-centered orthorhombic (fco) structure with equal interatomic distances $d_1=d_2=d_3$ inside the same molecular plane at about 75 GPa, as shown in Fig. 1(b). It is noted that the transition phenomenon found here is more important than the resultant structure (fco) because an incommensurate structure could not be obtained directly from our start-up *Cmca* structure with four bromine molecules by geometry optimization. The resultant fco structure is only an average structure of one incommensurate phase suggested before. We will discuss the phase in the following section.

The changes of the lattice constants and the interatomic distances in a molecular plane with pressure are shown in Fig. 3. We notice that the monotonic decrease of the lattice constants is interrupted and the differences among the three interatomic distances vanish at 75 GPa, revealing that the bromine molecule starts to dissociate. In Fig. 3, the experimental data measured by Fujihisa *et al.*[12] and the previous theoretical calculation by pseudopotential plane-wave method with GGA[19] are included. It can be seen that our results are in good agreement with the experimental data except those at 0 GPa. The slight underestimation of the lattice constants is mainly attributed to the zero temperature (static) calculations. The d_1 and d_3 are in agreement with the experimental results. Only d_2 is smaller than the experimental results except several data consistent with those of experiment. Moreover, it is noticed that our results are more accu-

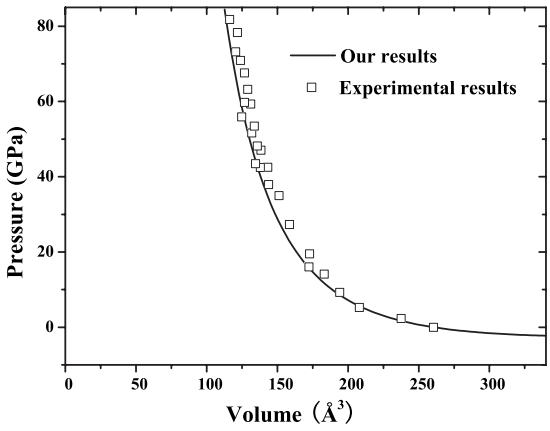

FIG. 2. Equation of states for the *Cmca* phase. Our results and the experimental data from Ref. 12 are presented by solid line and open squares, respectively.

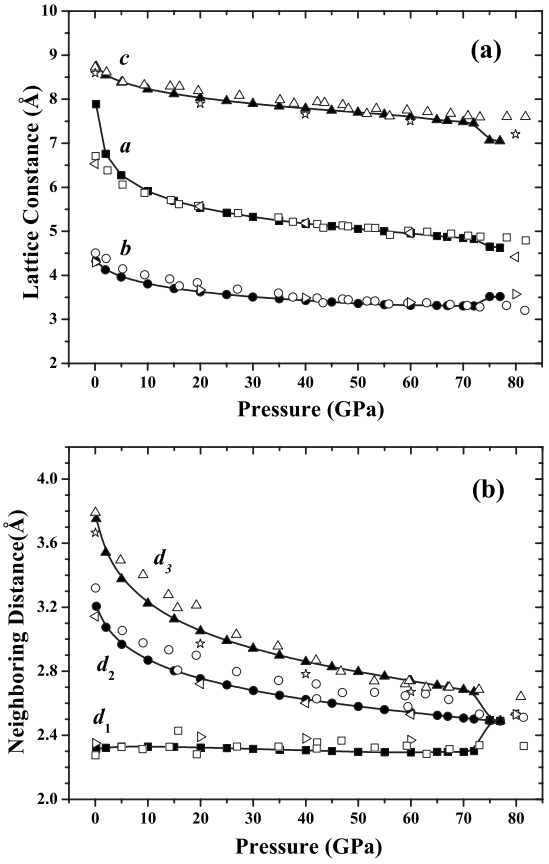

FIG. 3. Lattice constants and the interatomic distances inside the same molecular plane under various external pressures. Our results and the experimental data from Ref. 12 are presented by solid and open squares, circles, and up triangles in (a) and (b), respectively. The results of the previously theoretical calculations from Ref. 19 are denoted by open left triangles, right triangles, and open stars for comparison.

rate than those of the previous pseudopotential plane-wave method, because different GGA functional and optimization methods are used in our study.

Another phase transition from insulator to metal phase occurs at 55 GPa, which is in good agreement with the experimental value of 60 GPa. The band structure of solid molecular bromine under 0 and 55 GPa are presented in Fig. 4. The lines Σ, A, Λ, and H are the high symmetry axes in the first Brillouin zone of the base-centered-orthorhombic structure. The Σ and A axes are perpendicular to the layers of the molecular crystal, and the dispersion of the bands along these axes is governed by the interlayer interactions. The Λ and H axes are parallel to the layers. The dispersion of the conduction bands along the Γ-Σ-Y-H-T axes is much larger at 55 GPa than at 0 GPa. At zero pressure, the interaction between different planes is dominated by van der Waals-type potential. With increasing pressure, the interlayer distance decreases dramatically, which causes the intermolecular interaction between planes to be stronger and the band dispersion larger. Therefore, the metallization at low pressure is primarily attributed to the interlayer interaction.[16] From Fig. 4, one observes that the band gap is indirect and decreases

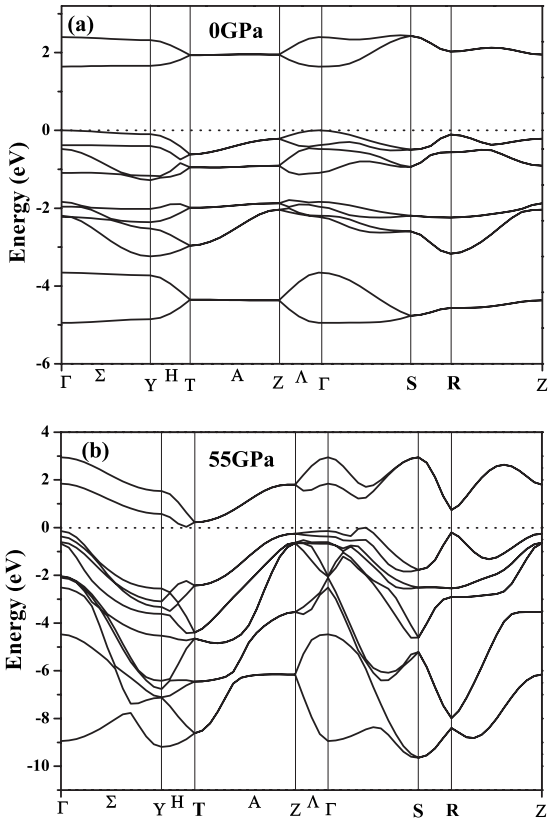

FIG. 4. Band structures of bromine under pressures of (a) 0 GPa and (b) 55 GPa.

with the increasing of pressure. The changes of the gap versus pressure are shown in Fig. 5. A gap closure can be clearly seen at about 55 GPa where the structure is still a molecular crystal with *Cmca* symmetry.

C. Intermediate phase with incommensurate structure

The quasihydrostatic powder x-ray diffraction measurements have clearly revealed that there is an intermediate phase with incommensurately modulated structure in solid

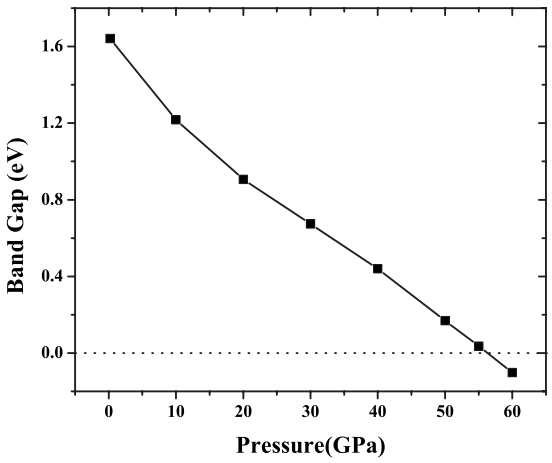

FIG. 5. The band gap vs pressure for bromine.

iodine above 23 GPa,[8] and a Raman scattering experiment suggested an incommensurate phase of bromine at a pressure region above 80 GPa.[9] However, there is not any x-ray diffraction experimental research on the structure of phase V for solid bromine up to now. For understanding the phase, a clue from the structure of phase V for iodine can be used, which is interpreted with a face-centered orthorhombic structure modulated with a modulation wave $k=(0.257,0,0)$.

Indeed, it has been a challenging problem for a long time to deal with the incommensurate structure from first-principles calculations based on periodic boundary conditions. However, such calculations can be performed by using commensurate analogs of the incommensurate structure approximately.[28] For example, recent calculations using the density functional theory have been performed for understanding the modulated phase of Se.[29] Here, we use a commensurate structure by a rational approximant with its modulation vector $k=(0.25,0,0)$ very close to the $k=(0.257,0,0)$ to mimic the incommensurate phase. A supercell of such a modulated structure is four times larger than the conventional cell of fco structure along the a axis. According to the harmonic modulation wave, atoms are displaced from their ideal positions along the b axis. The maximum displacement of modulations in the a-b plane is $B(y)=0.053$.[8] The modulated structure is orthorhombic with *Cmcm* symmetry shown in Fig. 1(c). The fco structure is only an average of such a modulated structure shown in Fig. 1(b), which is obtained by geometry optimization from the base-centered-orthorhombic structure (*Cmca*) directly.

Further geometry optimization shows that the maximum displacement of modulation in the a-b plane decreases with increasing pressure. So, the modulation reflections become weaker and disappear at 100 GPa where the modulated structure transforms into the monatomic phase II with symmetry *Immm*, as shown in Fig. 1(d). One notices that the transition pressure to phase II is in agreement with the experimental value of 115 GPa.

The enthalpies for the four phases (*Cmca*, modulated, fco, and bco) are shown in Fig. 6. The enthalpy of the fco phase is lower than that of the *Cmca* phase at about 75 GPa. However, the modulated phase has the lowest enthalpy in the pressure range from 65 to 100 GPa, suggesting that the phase transition from the *Cmca* to modulated phase may happen at a smaller pressure of 65 GPa, which is in excellent agreement with the most recent x-ray-absorption results.[10] We will discuss the phase transition in the next section deeply. The enthalpy of the bco phase shown in Fig. 6 is lower than that of modulated phase above 100 GPa, consistent with the result of geometry optimization.

For understanding the bonding behavior with pressure, we have analyzed the valance electronic charge density of the *Cmca* phase at 0 GPa [Fig. 7(a)] and 55 GPa [Fig. 7(b)] in the (100) plane. We also show the charge density of modulated phase at 80 GPa [Fig. 7(c)] and of bco phase at 105 GPa [Fig. 7(d)] in the (001) plane. At zero pressure, there are some electrons localized between the first neighboring atoms [Fig. 7(a)], which shows an obviously molecular bond character. Most of the electrons are located at the sides of atoms away from the bond, but there are no electrons in the intermolecular space. With increasing pressure, more and more electrons appear at the intermolecular space gradually, resulting in metallization [Fig. 7(b)]. The charge density around each atom is almost the same in Fig. 7(d), showing that phase II (bco structure) is a monatomic phase. On the other hand, the charge density in modulated structure [Fig. 7(d)] has some characters of both molecular and monatomic phases, so it should be an intermediate phase.

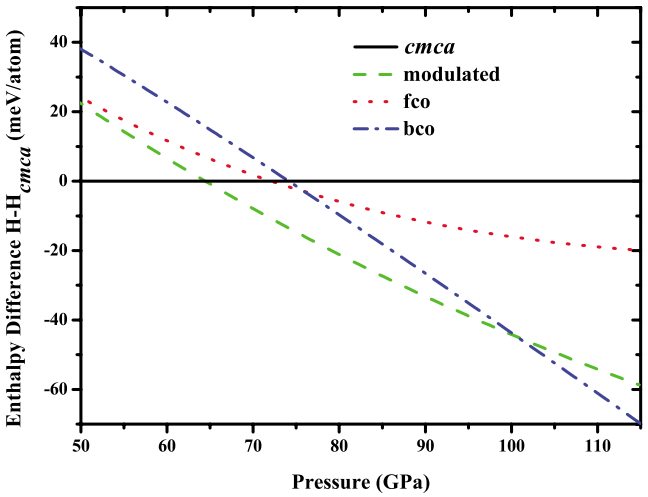

FIG. 6. (Color online) Calculated enthalpy differences of the four phases considered in this work as functions of pressure relative to that of the *Cmca* phase.

D. Mechanical stability of high-pressure phases and elastic properties

The elastic constants of materials describe its response to an applied stress, or conversely, the stress required to maintain a given deformation; the change of these values with pressure provides valuable information about the mechanical stability of the stressed lattice and mechanism of phase transition. Both stress and strain have three tensile and three shear components, giving six components in total. The linear elastic constants form a 6×6 symmetric matrix, having 27 independent components. For an orthorhombic crystal, the independent elastic stiffness tensor reduces to nine components C_{11}, C_{22}, C_{33}, C_{44}, C_{55}, C_{66}, C_{12}, C_{13}, and C_{23} in the Voigt notation. The well-known Born stability criteria[30] for orthorhombic system are

$$B_{1,ii}=C_{ii}>0 \quad (i=1-6),$$

$$B_{2,ij}=\begin{vmatrix} C_{ii} & C_{ij} \\ C_{ji} & C_{jj} \end{vmatrix}>0 \quad (\{ij\}=\{23\},\ \{31\},\ \text{or}\ \{12\}),$$

$$B_3=\begin{vmatrix} C_{11} & C_{12} & C_{13} \\ C_{21} & C_{22} & C_{23} \\ C_{31} & C_{32} & C_{33} \end{vmatrix}>0. \tag{2}$$

In the case of hydrostatic pressure, the C_{ij} (in the Voigt notation) is the elastic stiffness coefficient.

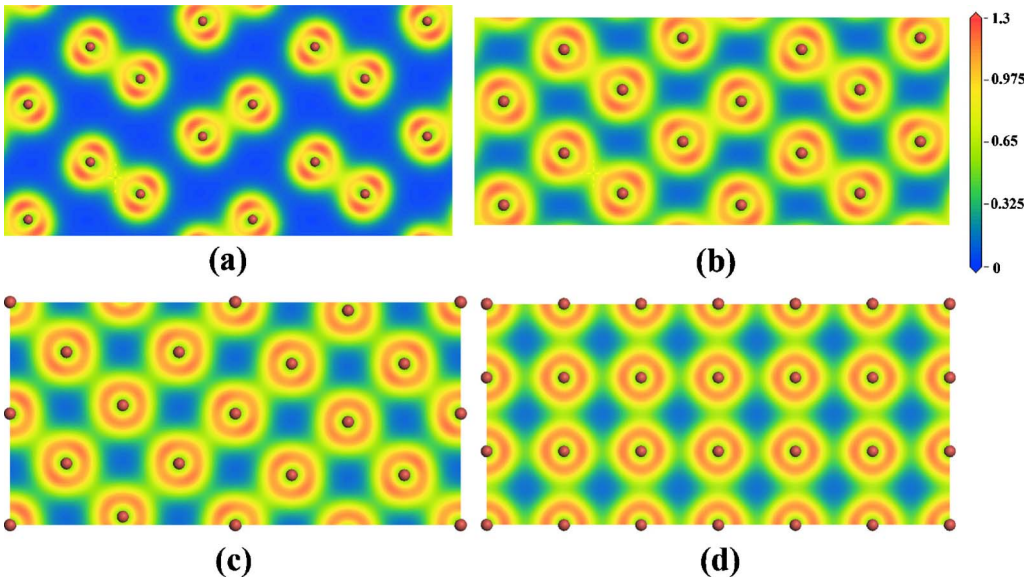

FIG. 7. (Color online) Distributions of charge density in the (100) plane of the *Cmca* phase at 0 and 55 GPa and in the (001) plane of the modulated phase at 80 GPa and bco phase at 105 GPa are shown in (a), (b), (c), and (d), respectively. There are 64 contour levels plotted with blue corresponding to 0 and red to 1.3 $e/\text{Å}^3$, as indicated in the scale bar.

The calculations have been performed for the *Cmca* phase under symmetry constraints. Our results show that both $B_{2,ij}$ and B_3 satisfy the Born stability criteria in the pressure range from 0 to 75 GPa; however, the Born stability criterion in $B_{1,ii}$ is violated at 75 GPa. As shown in Fig. 8, the elastic stiffness coefficients initially increase linearly, but C_{11}, C_{33}, and C_{44} start to soften above 55 GPa at which the insulator-to-metal transition occurs. It is noticed that the behavior of elastic properties is especially interesting in the vicinity of the phase transition. The elastic stiffness coefficients C_{11}, C_{33}, and C_{44} soften more rapidly with increasing pressure; especially, the shear elastic stiffness coefficient C_{44} eventually becomes zero at about 75 GPa, where the Born stability criterion is violated, implying that the structure is unstable and a phase transition happens. Moreover, a structural phase transition is clearly seen at 75 GPa from the change of atomic coordination. An abrupt increase in atomic coordination y at 75 GPa can be found in Fig. 9. From Fig. 3, we also notice that the significant change of the parameters in the b-c plane at this pressure dominates the structural phase transition. The instability of C_{44}, driving the transition from phase I (*Cmca*) to phase V (incommensurate), is related to the long wave librational $A_g^{(L)}$ mode softening above the metallization point.[9,17]

The elastic stiffness coefficients of the fco and modulated phases at 75 GPa are listed in Table II. It is significant that the shear elastic stiffness coefficient C_{66} is negative, suggesting that the fco structure is mechanically unstable. The instability of C_{66} indicates that the atoms in the a-b plane [shown in Fig. 1(b)] are not at stable sites. The modulation of atomic positions in the a-b plane along the b axis is a way to make

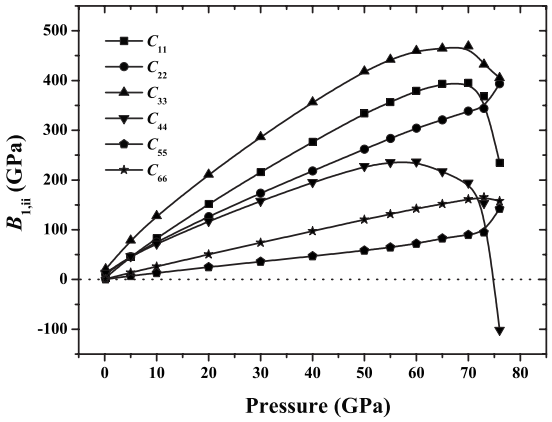

FIG. 8. Pressure dependence of Born coefficients $B_{1,ii}$ given by Eqs. (2) in the *Cmca* phase.

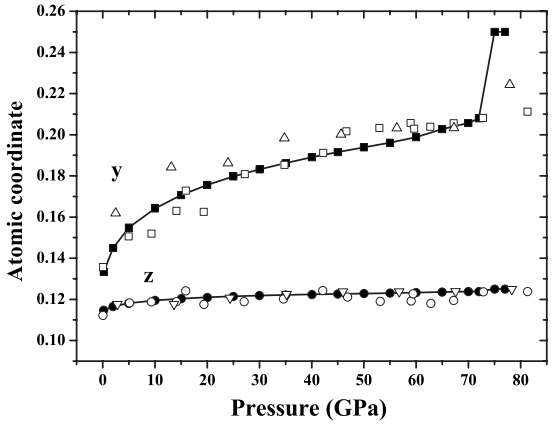

FIG. 9. The pressure dependence of the atomic coordinates (y,z). Our results and the experimental data from Ref. 12 are denoted by solid and open squares and circles, respectively, the linearized-muffin-tin-orbital results from Ref. 17 are shown by open up triangles and down triangles.

TABLE II. The calculated elastic stiffness coefficients (in GPa) of the fco and our modulated structure at 75 GPa.

Results	C_{11}	C_{22}	C_{33}	C_{44}	C_{55}	C_{66}	C_{12}	C_{13}	C_{23}
fco structure	417.00	418.56	232.57	140.57	146.10	−15.10	344.77	237.90	235.64
Modulated structure	379.89	385.60	273.85	144.75	135.89	94.05	341.55	245.76	226.52

the structure stable, reflected from the calculated elastic stiffness coefficients C_{ij} of our modulated structure which satisfy the Born stability criteria. As shown in Fig. 6, the enthalpy of the fco phase is lower than that of the *Cmca* phase at about 75 GPa. However, from our calculation of elastic stiffness coefficients, the fco phase is mechanically unstable. The stable phase should be the modulated phase which has the lowest enthalpy in the pressure range. On the other hand, the modulated phase has lower enthalpy than the *Cmca* phase above 65 GPa. So, it is possible that the phase transition begins at about 65 GPa and completes at 75 GPa where the *Cmca* phase becomes unstable. The *Cmca* and the modulated phases may coexist in the pressure range from 65 to 75 GPa. This result is consistent with the most recent extendent x-ray-absorption fine structure experimental research,[10] which shows that a phase transition happens at 65±5 GPa possibly, and a mixture of the *Cmca* phase with the incommensurately modulated structure appears in the phase transition domain.

E. Comparison of x-ray diffraction patterns

The high-pressure x-ray powder diffraction experiments had been carried out on the molecular phase of bromine.[12,31] The x-ray powder diffraction patterns above 80 GPa had also been reported, but they were indexed to be the body-centered orthorhombic structure[12,31] which conflicts with the incommensurate structure suggested by the Raman spectroscopy experiment.[9] Here, we compare the x-ray diffraction patterns of our structures with the experimental ones to gain some information. Theoretical x-ray diffraction patterns are obtained by using the module of the Reflex in Materials Studio with the same x-ray wavelength of 0.6199 Å as the experimental one.

Figure 10(a) shows the x-ray diffraction pattern of our calculated structure at 70 GPa. The arrows indicate the experimental peaks of bromine at 70 GPa.[12] We note that the peaks before $2\theta=25°$ are very similar between the experiment and theory. The main peaks from $2\theta=25°$ to 30° are similar except that several weak peaks are missing in experimental data. Maybe these peaks are too weak to be observed in experiment. The x-ray diffraction pattern of our calculated structure at 70 GPa is in an excellent agreement with the experimental pattern.

Figure 10(b) shows the x-ray diffraction pattern of our modulated structure of bromine at 80 GPa. The arrows show the experimental peaks of bromine at 88 GPa from Ref. 31, and these peaks are consistent with the main peaks of our modulated structure. For comparison, we also show the satellite reflection peaks of incommensurate phase of iodine[8] labeled by asterisks in the same figure. It is found that the first peak should be the first satellite reflection peak in the incommensurate structure, which is very important in the determination of the structure of Br-V, but it was not indexed in the experimental work. The fourth peak should be the second satellite reflection peak, which was occulted by the reflection from the gasket in experiment.[31] Furthermore, the multiple peaks around 20° and 26° are too broad and merge together in the experimental work. Therefore, the Br-V should be an incommensurate structure which closely resembles our modulated structure rather than the body-centered orthorhombic structure. More x-ray diffraction experimental studies are needed for further understanding of this phase.

IV. CONCLUSIONS

In summary, three pressure-induced phase transitions in solid bromine have been obtained up to 100 GPa. The insulator-metal transition due to band overlap is found at about 55 GPa, which is in good agreement with the experimental observation. The transition from the *Cmca* phase to the incommensurate phase happens in the pressure range from 65 to 75 GPa where the shear elastic stiffness coefficient C_{44} of the *Cmca* phase softens to zero at 75 GPa,

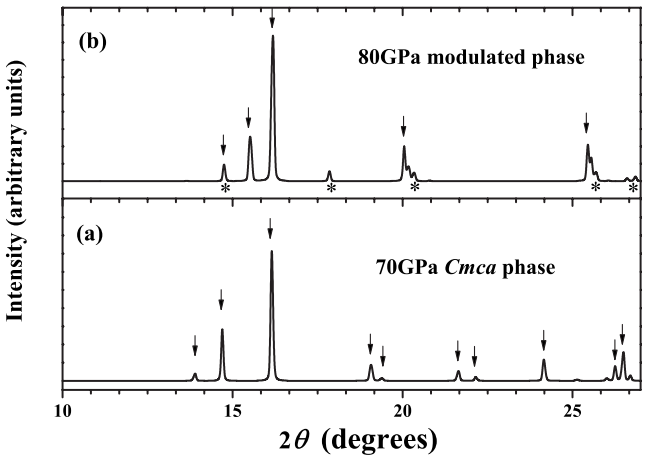

FIG. 10. Powder x-ray diffraction pattern of our calculated structure of solid bromine at (a) 70 GPa and (b) 80 GPa. The arrows in (a) indicate the experimental peaks of bromine in the *Cmca* phase at 70 GPa from Ref. 12. The arrows in (b) show the experimental peaks of bromine at 88 GPa from Ref. 31. The asterisks in (b) indicate the satellite reflection peaks of incommensurate phase of iodine at 24.6 GPa from Ref. 8.

indicating that the shear instability induces the phase transition. On the basis of a comparison of x-ray diffraction patterns, enthalpy, and elastic stiffness coefficients, it is found that the structure of bromine phase V is close to our modulated structure with modulation wave vector around (0.25, 0, 0). The transition from phase V (modulated structure) to phase II (bco structure) occurs at 100 GPa, which is in agreement with the result of the Raman scattering experiment.

ACKNOWLEDGMENTS

This work was supported by the National Natural Science Foundation of China under Grants No. 10574053 and No. 10674053, 2004 NCET and 2003 EYTP of MOE of China, National Basic Research Program of China, Grant No. 2005CB724400, and The Cultivation Fund of the Key Scientific and Technical Innovation Project No. 2004-295.

*Author to whom correspondence should be addressed: cuitian@jlu.edu.cn

[1] R. J. Nelmes, D. R. Allan, M. I. McMahon, and S. A. Belmonte, Phys. Rev. Lett. **83**, 4081 (1999).
[2] M. I. McMahon, O. Degtyareva, and R. J. Nelmes, Phys. Rev. Lett. **85**, 4896 (2000).
[3] U. Schwarz, L. Akselrud, H. Rosner, A. Ormeci, Y. Grin, and M. Hanfland, Phys. Rev. B **67**, 214101 (2003).
[4] C. Hejny and M. I. McMahon, Phys. Rev. Lett. **91**, 215502 (2003).
[5] M. I. McMahon, C. Hejny, J. S. Loveday, L. F. Lundegaard, and M. Hanfland, Phys. Rev. B **70**, 054101 (2004).
[6] C. Hejny, L. F. Lundegaard, S. Falconi, M. I. McMahon, and M. Hanfland, Phys. Rev. B **71**, 020101 (2005).
[7] O. Degtyareva, E. Gregoryanz, M. Somayazulu, H. K. Mao, and R. J. Hemley, Phys. Rev. B **71**, 214104(R) (2005).
[8] K. Takemura, K. Sato, H. Fujihisa, and M. Onoda, Nature (London) **423**, 971 (2003).
[9] T. Kume, T. Hiraoka, Y. Ohya, S. Sasaki, and H. Shimizu, Phys. Rev. Lett. **94**, 065506 (2005).
[10] A. San-Miguel, H. Libotte, M. Gauthier, G. Aquilanti, S. Pascarelli, and J. P. Gaspard, Phys. Rev. Lett. **99**, 015501 (2007).
[11] B. M. Riggleman and H. G. Drickamer, J. Chem. Phys. **38**, 2721 (1963).
[12] H. Fujihisa, Y. Fujii, K. Takemura, and O. Shimomura, J. Phys. Chem. Solids **56**, 1439 (1995).
[13] Y. Fujii, K. Hase, T. Ohishi, N. Hamaya, and A. Onodera, Solid State Commun. **59**, 85 (1986).
[14] Y. Fujii, K. Hase, N. Hamaya, Y. Ohishi, A. Onodera, O. Shimomura, and K. Takemura, Phys. Rev. Lett. **58**, 796 (1987).
[15] R. Reichlin, A. McMahon, M. Ross, S. Martin, J. Hu, R. Hemley, H. Mao, and Y. Wu, Phys. Rev. B **49**, 3725 (1994).
[16] N. Orita, K. Niizeki, K. Shindo, and H. Tanaka, J. Phys. Soc. Jpn. **61**, 4502 (1992).
[17] H. Miyagi, K. Yamaguchi, H. Matsuo, and K. Mukose, J. Phys.: Condens. Matter **10**, 11203 (1998).
[18] K. Yamaguchi and H. Miyagi, Phys. Rev. B **57**, 11141 (1998).
[19] M. S. Miao, V. E. Van Doren, and Jose Luis Martins, Phys. Rev. B **68**, 094106 (2003).
[20] M. Segall, P. Lindan, M. Probert, C. Pickard, P. Hasnip, S. Clark, and M. Payne, J. Phys.: Condens. Matter **14**, 2717 (2002).
[21] T. H. Fischer and J. Almlof, J. Phys. Chem. **96**, 9768 (1992).
[22] J. P. Perdew, K. Burke, and M. Ernzerhof, Phys. Rev. Lett. **77**, 3865 (1996).
[23] H. J. Monkhorst and J. D. Pack, Phys. Rev. B **13**, 5188 (1976).
[24] S. S. Batsanov, Inorg. Mater. **37**, 871 (2001).
[25] R. W. G. Wyckoff, *Crystal Structures*, 2nd ed. (Interscience, New York, 1963), p. 52.
[26] A. Pasternak, A. Anderson, and J. W. Leech, J. Phys. C **11**, 1563 (1978).
[27] F. Brich, J. Geophys. Res. **83**, 1257 (1978).
[28] M. I. McMahon and R. J. Nelmes, Chem. Soc. Rev. **35**, 943 (2006).
[29] G. J. Ackland and H. Fox, J. Phys.: Condens. Matter **17**, 1851 (2005).
[30] M. Born and K. Huang, *Dynamical Theory of Crystal Lattices* (Clarendon, Oxford, 1956).
[31] Y. Fujii, K. Hase, Y. Ohishi, H. Fujihisa, N. Hamaya, K. Takemura, O. Shimomura, T. Kikegawa, Y. Amemiya, and T. Matsushita, Phys. Rev. Lett. **63**, 536 (1989).